# Structural and functional brain abnormalities in HIV disease revealed by multimodal MRI fusion: association with cognitive function

Jing Sui[#a,b,c], Xiang Li[#b,c], Ryan P. Bell[d], Sheri L. Towe[d], Syam Gadde[e], Nan-kuei Chen[e,f], Christina S. Meade[d,e]

[a] Tri-Institutional Center for Translational Research in Neuroimaging and Data Science, Georgia State University, Georgia Institute of Technology, and Emory University, Atlanta, GA, USA

[b] National Laboratory of Pattern Recognition, Institute of Automation, Chinese Academy of Sciences, Beijing, China

[c] University of Chinese Academy of Sciences, Center for Excellence in Brain Science and Intelligence Technology, Beijing, China

[d] Department of Psychiatry & Behavioral Sciences, Duke University School of Medicine, Durham, NC, United States

[e]Brain Imaging and Analysis Center, Duke University, Durham, NC, United States

[f] Department of Biomedical Engineering, University of Arizona College, Tucson, AZ, United States

[#]Xiang Li and Jing Sui equally contributed to this work.

Corresponding author
Christina S. Meade, PhD
Duke University Box 102848
Durham, NC 27708, USA
919-613-6549
christina.meade@duke.edu

Summary: This study applied 3-way supervised MRI fusion to investigate structural and functional co-alterations in the brain in adults with and without HIV. One joint multimodal component was both group discriminating and correlated with cognitive function across all modalities.

## ABSTRACT

**Background**: HIV-associated neurocognitive impairment remains a prevalent comorbidity that impacts daily functioning and increases morbidity. While HIV infection is known to cause widespread disruptions in the brain, different MRI modalities have not been effectively integrated. This study applied 3-way supervised fusion to investigate how structural and functional co-alterations affect cognitive function.

**Methods**: Participants (59 with HIV and 58 without HIV) completed comprehensive neuropsychological testing and multimodal MRI scanning to acquire high-resolution anatomical, diffusion-weighted, and resting-state functional images. Pre-processed data was reduced using voxel-based morphometry, probabilistic tractography, and regional homogeneity, respectively. We applied multimodal canonical correlation analysis with reference plus joint independent component analysis (MCCAR+jICA), using global cognitive functioning as the reference.

**Results**: Compared to controls, participants with HIV had lower global cognitive functioning. One joint component was both group discriminating and correlated with cognitive function. This component included the following covarying regions: fractional anisotropy in the corpus callosum, short and long association fiber tracts, and corticopontine fibers; gray matter volume in thalamus, prefrontal cortex, precuneus, posterior parietal regions, and occipital lobe; and functional connectivity in fronto-parietal and visual processing regions. Component loadings for fractional anisotropy also correlated with immunosuppression.

**Conclusions**: These results suggest that co-alterations in brain structure and function can distinguish people with and without HIV and may drive cognitive impairment. As MRI becomes more commonplace in HIV care, multimodal fusion may provide neural biomarkers to support diagnosis and treatment of cognitive impairment.

Key words: neuroHIV; magnetic resonance imaging; multimodal fusion

## INTRODUCTION

With the advent of combination antiretroviral therapies, people with HIV (PWH) have nearly average life expectancies [1]. Yet, HIV-associated neurocognitive disorder (HAND) remains a prevalent comorbidity, with rates ranging from 15% to 55% across populations [2]. While milder forms of HAND now predominate, these impairments have real-world impacts on daily functioning (e.g., employment, medication adherence) and are predictive of increased morbidity and mortality [3]. Even with sustained viral suppression, HIV reservoirs in the central nervous system may lead to brain injury via chronic inflammation [4].

Noninvasive magnetic resonance imaging (MRI) has yielded important insights into the neuropathology of HIV. Structural MRI studies that quantify gray matter morphology have demonstrated HIV-related atrophy predominantly in the frontal lobes and striatum [5]. Diffusion-weighted imaging (DWI), which maps the diffusion of water molecules across white matter, has revealed decreased integrity of multiple projection, association, and callosal fibers in PWH compared to HIV-negative controls [6]. Studies of resting-state functional MRI (rs-fMRI), which measures the temporal correlation of spontaneous changes in blood flow across spatially distributed regions, have reported diminished connectivity within and between major neural networks in PWH [7]. While there is no specific profile of neuroHIV, likely due to multiple mechanisms, the growing literature supports the role of brain abnormalities in the development of HAND.

While each MRI modality offers unique and complementary information related to neurologic disease, when evaluated independently, unimodal studies may provide an incomplete characterization of brain structure and function. By contrast, innovative fusion approaches jointly analyze multiple neuroimaging datasets to reveal interrelated patterns

across modalities. Specifically, multimodal canonical correlation analysis with reference plus joint independent component analysis (MCCAR+jICA) is a fusion method that flexibly captures multimodal interactions and generates independent spatial components [8]. This analytic framework has been successfully applied to examine cognitive dysfunction related to multiple neuropsychiatric disorders, exhibiting superior estimation accuracy and reliability relative to its alternatives [9, 10].

To date, MRI studies in neuroHIV have not been adequately integrated to yield a comprehensive view of the structural and functional co-alterations associated with neurocognitive impairment. The aim of this project was to identify neural biomarkers acquired using multimodal MRI that are predictive of cognitive function in PWH. Given the complexity of high-dimensional datasets, our supervised model used cognitive function as a reference to identify linked multimodal components.

## METHODS

### Sampling

Adults aged 18-55 years were recruited from infectious diseases clinics and the community via advertisements in local newspapers, websites, and nonprofit organizations. For individuals with known HIV diagnosis, HIV status was verified by medical record review. PWH had to have been diagnosed for >3 months and prescribed antiretroviral medications. For others, an oral rapid antibody test (OraSure ADVANCE® HIV-1/2) was conducted; all HIV-negative participants had a non-reactive result. Exclusion criteria were: English non-fluency or illiteracy; <8$^{th}$ grade education; severe learning disability; unresolved neurological disorders or neuroinfections; severe head trauma with loss of consciousness >30 minutes and persistent functional decline; bipolar I or psychotic disorder; acute psychiatric symptoms interfering with functioning; MRI contraindications; and/or impaired mental

status. Current nicotine, alcohol, and marijuana use was permissible, but participants could not meet criteria for dependence. For other drugs, individuals were excluded for a history of dependence, lifetime regular use for >2 years, any use in the past 30 days, and/or a positive urine drug screen. These exclusions are consistent with current guidelines for classifying contributing and confounding conditions to HAND [11].

**Procedures**

Participants were enrolled in one of three protocols with shared procedures. The proportion of PWH was equivalent across protocols (55%, 47%, and 50%; $\chi(2)^2$=0.42, p=.81). Participants provided written informed consent, and procedures were approved by the institutional review board at Duke University Health System. An in-person screening assessed medical, psychiatric, and substance abuse histories. Eligible participants returned for neuropsychological testing, MRI scanning, and additional assessments. Participants abstained from alcohol, marijuana, and illicit drugs for ≥4 hours prior to the visit. To minimize nicotine withdrawal, participants were allowed to smoke up to 30 minutes prior to the MRI.

**Assessments**

***Screening***. The Addiction Severity Index-Lite, a structured clinical interview, assessed current and lifetime functioning across multiple domains, including substance use, psychiatric symptoms, and medical conditions [12]. The Mini International Neuropsychiatric Interview identifed DSM-IV mood and psychotic disorders [13]. Module E of the Structured Clinical Interview for DSM-IV identified substance use disorders [14]. Recent drug use was assessed using a urine toxicology screen for amphetamine, barbiturates, benzodiazepines, cannabis, cocaine, methadone, methamphetamine, opioids, and oxycodone. Medical records were reviewed to ensure no exclusionary conditions.

***Neuropsychological testing***. The battery assessed seven domains relevant to HAND, including executive functioning, processing speed, working memory, verbal fluency, learning, motor, and memory (see **Supplementary Table 1** for description of tests). Raw scores were converted to standardized T-scores (M= 50, SD= 10) that correct for age and, when available, other demographic factors. T-scores for each test within a domain were averaged to create a domain T-score, and domain T-scores were averaged to create a global T-score.

***HIV clinical data***. The following data were abstracted from the medical record: date of HIV diagnosis, nadir and current $CD4^+$ T-cell count, current antiretroviral regimen, and most recent HIV viral load. All participants had lab testing within 8 months of their MRI (M=2.03 months, SD=1.71). Viral suppression was defined as <50 copies/mL. To normalize the data for analysis, $CD4^+$ T-cell counts were square root transformed.

**MRI data acquisition**

Data were acquired with a single 3.0T GE Discovery MR750 whole-body scanner using an 8-channel head coil. High-resolution T1-weighted (T1w) structural images were acquired with the following parameters: TR=8.10ms, TE=3.18ms, FOV=25.6cm, 256*256 matrix, 12° flip, 166 interleaved slices of 1mm thickness). DWI was acquired in the axial plane using single-shot spin-echo echo-planar imaging (FOV=25.6cm, 128*128 matrix, $90^o$ flip, 2mm interleaved slices). Additional parameters differed slightly between protocol 1 (b-factor=900 s/$mm^2$, TR/TE=10,000/83.2ms, 73 slices), protocol 2 (b-factor=800 s/$mm^2$, TR/TE=8000/77.9ms, 67 slices), and protocol 3 (b-factor=800 s/$mm^2$, TR/TE=8000/78.2ms, 67 slices). Data were acquired in 30 directions for the first two protocols and 64 directions for the third protocol. The 64-direction protocol was downsampled using a MATLAB dot() function (inner product) that identified the diffusion-encoding direction most similar to

those in the 30-direction protocol. For the rs-fMRI data, whole-brain BOLD images were collected using T2*-weighted echo-planar imaging (TR=2000ms, FOV=24cm, 64*64 matrix, 3.8mm interleaved slices, voxel size 3.75*3.75mm*3.8mm). Additional parameters differed slightly between the first protocol (TE=27ms, 77° flip, 39 slices) and the other two protocols (TE=25ms, 90° flip, 35 slices). Data harmonization consisted of ensuring that all scans had 148 volumes.

**Image preprocessing**

The DWI data was denoised [15], motion and eddy-corrected using DTIPrep 3.1 [16], and preprocessed using tools from FSL 5.0.9 (B1 bias-correction, global DWI intensity normalization, rigid-body registration between participants' mean B0 images and T1w data, and non-linear registration between T1w data and the standard MNI brain) [17]. Probabilistic tractography was conducted in MRtrix 3.0 using an anatomically-constrained procedure and a diffusion tensor. One million tracks were generated by seeds from the mask image in 0.2mm steps [18, 19]. Fractional anisotropy (FA) was then calculated within all white matter voxels.

The T1w images were skull-stripped using custom thresholds and analyzed with FSL-VBM [20]. Participant-level maps of gray matter volume (GMV) were created.

For rs-fMRI, the first six volumes were excluded to ensure steady-state sampling. Data processing was conducted using FSL, including motion correction using rigid-body transformation, slice-timing correction, high-pass temporal filtering using a Gaussian filter at 0.01Hz, and signal intensity normalization. White matter and cerebrospinal fluid means were regressed out. Motion and physiological-related components were removed using ICA-AROMA [21]. Images were registered to the 2-mm MNI template using nonlinear registration [22]. Registration of functional data to the T1w acquisition was done using a 12-

parameter affine transformation. After pre-processing and warping to MNI space, regional homogeneity (ReHo) was calculated using the AFNI v20.2.16 tool 3dReHo utilizing a 27-voxel neighborhood [23]. ReHo evaluates the similarity between the time series of a voxel to a predefined cluster of its nearest neighbors [24].

**Statistical analysis**

***Feature normalization***. Images were upsampled to $3\mathrm{mm}^3$ and spatially smoothed using a Gaussian kernel with a full width at half maximum of $6\mathrm{mm}^3$. The three-dimensional images were reshaped into a one-dimensional vector and stacked, forming a matrix ($\mathrm{N}_{\mathrm{participant}} \times \mathrm{N}_{\mathrm{voxel}}$) for each modality. The matrices were normalized to have the same average sum of squares. A single normalization factor was used for each data type; thus, the relative scaling within a given data type was preserved, but the units between data types were the same (in a least-squares sense). Age, intracranial volume, nicotine use, and protocol were regressed out from the ReHo, GMV, and FA features.

***Multimodal fusion***. The preprocessed MRI features were fed into the MCCAR+jICA pipeline with Global T score as the reference (**Figure 1**). After MCCAR optimization, we obtained the canonical variants that were most correlated with the reference in each modality and across participants between modalities. Joint ICA was applied to the concatenated maps to keep the modality linkage while maximizing the spatial independence of components. Based on the minimum description length criterion [25], 23 independent components (ICs) were estimated with corresponding participant-wise loadings derived for each modality. ICs from the same index across all three modalities are considered joint ICs. Our analysis selected the joint IC, denoted $\mathrm{IC}_{\mathrm{ref}}$, that correlated maximally with the reference across all modalities [8]. Multivariate analysis of variance (MANOVA) was used to compare the groups on the $\mathrm{IC}_{\mathrm{ref}}$ loadings. The identified brain regions are described using

the Harvard-Oxford Atlas for gray matter regions [26] and the IIT Human Brain Atlas for white matter tracts [27]. Pearson correlation examined the relationship between $IC_{ref}$ loadings and $CD4^+$ T-cell counts, and independent sample t-tests compared loadings by HIV suppression.

## RESULTS

### Participant characteristics

**Table 1** describes the demographic characteristics of the 59 PWH and 58 HIV-negative controls. The majority of PWH were on a regimen of dual nucleoside reverse transcriptase inhibitor plus either a non-nucleoside reverse transcriptase inhibitor (42.4%), an integrase strand transfer inhibitor (33.9%), or a protease inhibitor (15.3%); 8.5% were on a different combination. Duration since HIV diagnosis ranged from 4 months to 29 years (Mdn=7.17, IQR=11.70). The median nadir $CD4^+$ T-cell count was 250 (IQR=297), and 41% had a nadir <200. Currently, the majority (80%) had a suppressed plasma HIV RNA, and the median $CD4^+$ T-cell count was 598 (IQR=424). Participants with unsuppressed viral load were significantly more likely to have a current $CD4^+$ T-cell count <200 (67% vs. 0%; $\chi^2(1)=36.25$, $p<.001$). PWH were older and more likely to smoke cigarettes daily, but they were otherwise comparable to the HIV-negative group. As expected, cognitive functioning was significantly lower in PWH compared to those without HIV.

### Joint independent component

**Figure 2** displays representative spatial maps for $IC_{ref}$ , the joint component that maximally correlated with global T score across all three modalities. This component was characterized by the following linked regions: FA in bilateral corpus callosum (splenium, body, and genu), short and long association fiber tracts, and corticopontine fibers; GMV in bilateral visual cortex, medial orbitofrontal cortex, posterior parietal cortex, and thalamus;

and ReHo in bilateral posterior parietal cortex, dorsomedial and ventromedial prefrontal cortex, precuneus, precentral and postcentral gyri, and visual cortex. **Supplementary Table 2** details the regions comprising the component. As shown in **Figure 2**, $IC_{ref}$ correlated significantly with global T score for FA, GMV, and ReHo.

There was a significant group difference for $IC_{ref}$ [F (3, 113)=2.985, p=.034; Wilk's Λ=.927]. PWH had lower loadings compared to HIV-negative controls for FA and GMV, meaning the component was expressed less strongly (**Table 2**).

**Association with HIV clinical measures**

For $IC_{ref}$, markers of immunosuppression correlated with the component loading for FA, but not GMV or ReHo. Specifically, lower FA loadings correlated with lower current (r=.272, p=.037) and nadir (r=.338, p=.009) $CD4^+$ T-cell counts. In contrast, HIV viral suppression was unrelated to $IC_{ref}$ loadings.

In a sensitivity analysis excluding participants with unsupressed HIV, there were similar group differences in $IC_{ref}$ loadings for FA [F(1,103=4.922, p=.029] and GMV [F(1,103)=5.606, p=.020]. However, the correlation between FA loadings and $CD4^+$ T-cell counts were no longer significant for current (r=.124, p=.406) or nadir (r=.268, p=.068) with the restricted range.

## DISCUSSION

By applying an innovative analytic approach that "fuses" multimodal MRI data, we identified co-alterations in brain structure and function that correlated with cognitive function. Specifically, global T score was linked to reduced volume in the thalamus and visual, posterior parietal, and orbitofrontal cortices, reduced white matter integrity throughout the corpus callosum and association fibers, and altered activity in frontal-parietal and occipital networks.

PWH had lower component scores for both FA and GMV, suggesting that HIV-associated alterations in brain structure drive neurocognitive impairment. A unique feature of multimodal fusion is its ability to discover linked alterations in spatially distinct brain regions, even when there is no direct morphologic connection. Building upon a literature dominated by unimodal analyses, our results support the role of diffuse co-alterations in brain structure and function in neuroHIV [5-7].

Supporting a linkage between white and gray matter structure, we found HIV-associated reductions in thalamic volume and integrity of thalamic projection fibers correlated with worse cognitive function. The thalamus is a major "hub" region that acts as a relay station between subcortical areas and the cerebral cortex [28]. Prior DWI studies in PWH have documented microstructural abnormalities in the white matter fibers of the thalamus [29-31], while structural MRI studies have identified HIV-related atrophy in adjacent gray matter [5].

Effective neural communication may be constrained by the structural composition of the brain. The ReHo component linked to cognitive function displayed activations in posterior parietal and prefrontal cortices, regions typically associated with executive function [33], with corresponding deactivations in the precuneus and medial prefrontal cortex. Such divergent activity in neural function is characteristic of healthy cognition [34]. This pattern of local functional connectivity was linked to reduced integrity in the corpus callosum, a white matter fiber that forms interhemispheric connections, and reduced volume in major hubs including the thalamus and precuneus. In addition, we found both functional and structural abnormalities in visual processing regions that were negatively correlated with global cognitive function. While there were no group differences for ReHo, the overall component loading may have masked abnormalities in the neural activation patterns linked to cognitive

function, as HIV has been associated with both hypoactivation in hippocampal and visual processing regions and compensatory hyperactivation in fronto-striatal regions to preserve cognitive function [35]. Future studies might consider the potentially divergent implications of positive versus negative functional homogeneity in relation to HIV-associated neurocognitive impairments.

Clinically, our results suggest that HIV-related immunosuppression may increase vulnerability to white matter degradation, consistent with unimodal studies [5, 36]. The FA component was correlated with both nadir and current $CD4^+$ T-cell counts, such that participants with greater immunosuppression had reduced white matter integrity. While the so-called legacy effect linking historical severe immunosuppression with brain structure and cognitive function has been widely reported [2, 3, 7], our results underscore the neurologic benefit of restoring and maintaining strong immune function. Unsuppressed viral load was unrelated to the joint component, and differences in brain structure linked to cognitive function were observed even when excluding people with unsuppressed HIV. Prior studies have consistently found that viral load is a poor predictor of brain integrity, which may result from cumulative inflammatory processes [37]. However, we were unable to tease out the extent to which immunosuppression during periods of untreated HIV may be driving our findings. In contrast, GMV and ReHo metrics in the identified multimodal component were unrelated to HIV disease characteristics, suggesting that degradations in white matter may precede alterations in gray matter regions, possibly serving as an early marker of HAND [38].

Despite the innovative analytic approach and robust findings, the following limitations should be mentioned. First, the reference-guided fusion strategy utilizes selected MRI features rather than original data (e.g., using ReHo instead of 4D fMRI data). Since the time series of the fMRI data were not used, there may have been some loss of the temporal

information. However, compared to the high-dimensional raw data, features tend to be more tractable and provide a more concise signature to link [39, 40]. Future investigations may wish to incorporate alternative features such as mean diffusivity, cortical thickness, and task-evoked neural activation. Another potential limitation is the cross-sectional design. Longitudinal analyses are needed to verify the temporal relationship between structural and functional changes in the brain and their causal relationship to cognitive impairment in larger samples of PWH with more generalizable eligibility criteria. Finally, the MMCAR+jICA framework was designed to identify brain regions that maximally covary across modalities and that strongly correlate with the reference. There may be additional HIV-related alterations in one or more MRI modalities that were not revealed by this approach because they are unrelated to cognitive function or are not linked across modalities.

In summary, our innovative supervised data fusion approach revealed multimodal neural signatures of HIV that correlated with cognitive function. To the best of our knowledge, this is the first attempt to holistically investigate the impact of brain function and structure on HIV-associated neurocognitive impairment. Given that cognitive decline in PWH is associated with increased morbidity and mortality, there is a critical need for accurate biomarkers of HAND to aid diagnosis, treatment planning, and long-term monitoring. The current standard for HAND diagnosis involves lengthy neuropsychological testing that can lack precision and sensitivity. Multimodal fusion, which reveals covariation across imaging and clinical modalities, holds great promise as a more reliable and cost-effective biomarker of HAND.

**ACKNOWLEDGMENTS**

We thank all of the participants who were part of the original studies and the research staff who assisted with data collection.

**FUNDING**

This work was supported by the National Institute on Drug Abuse at the National Institutes of Health [R01-DA045565]. The content is solely the responsibility of the authors and does not necessarily represent the official views of the National Institutes of Health.

**POTENTIAL CONFLICTS**

All authors declare that they have no conflicts of interest.

## REFERENCES


1. Marcus JL, Chao CR, Leyden WA, et al. Narrowing the Gap in Life Expectancy Between HIV-Infected and HIV-Uninfected Individuals With Access to Care. J Acquir Immune Defic Syndr **2016**; 73(1): 39-46.
2. Saylor D, Dickens AM, Sacktor N, et al. HIV-associated neurocognitive disorder - pathogenesis and prospects for treatment. Nat Rev Neurol **2016**; 12(5): 309.
3. Alford K, Vera JH. Cognitive Impairment in people living with HIV in the ART era: A Review. Br Med Bull **2018**; 127(1): 55-68.
4. Carroll A, Brew B. HIV-associated neurocognitive disorders: recent advances in pathogenesis, biomarkers, and treatment. F1000Research **2017**; 6: 312.
5. Israel SM, Hassanzadeh-Behbahani S, Turkeltaub PE, Moore DJ, Ellis RJ, Jiang X. Different roles of frontal versus striatal atrophy in HIV-associated neurocognitive disorders. Hum Brain Mapp **2019**; 40(10): 3010-26.
6. Chang L, Shukla DK. Imaging studies of the HIV-infected brain. In: Brew BJ. Handbook of Clinical Neurology Vol. 152: Elsevier, **2018**:229-64.
7. Hakkers CS, Arends JE, Barth RE, Du Plessis S, Hoepelman AI, Vink M. Review of functional MRI in HIV: effects of aging and medication. J Neurovirol **2017**; 23(1): 20-32.
8. Qi S, Calhoun VD, van Erp TGM, et al. Multimodal Fusion With Reference: Searching for Joint Neuromarkers of Working Memory Deficits in Schizophrenia. IEEE Trans Med Imaging **2018**; 37(1): 93-105.
9. Qi S, Yang X, Zhao L, et al. MicroRNA132 associated multimodal neuroimaging patterns in unmedicated major depressive disorder. Brain **2018**; 141(3): 916-26.
10. Sui J, Qi S, van Erp TGM, et al. Multimodal neuromarkers in schizophrenia via cognition-guided MRI fusion. Nature Communications **2018**; 9(1): 3028.
11. Antinori A, Arendt G, Becker JT, et al. Updated research nosology for HIV-associated neurocognitive disorders. Neurology **2007**; 69(18): 1789-99.

12. McLellan AT, Kushner H, Metzger D, et al. The Fifth Edition of the Addiction Severity Index. J Subst Abuse Treat **1992**; 9(3): 199-213.
13. Sheehan DV, Lecrubier Y, Sheehan KH, et al. The Mini-International Neuropsychiatric Interview (M.I.N.I.): the development and validation of a structured diagnostic psychiatric interview for DSM-IV and ICD-10. J Clin Psychiatry **1998**; 59 Suppl 20(Suppl 30): 22-33;quiz 4-57.
14. First MB, Spitzer RL, Gibbon M, Williams JBW. Structured Clinical Interview for DSM-IV Axis I Disorders, Research Version, Patient/Non-patient Edition. New York: Biometrics Research, New York State Psychiatric Institute, **1996**.
15. Chen NK, Chang HC, Bilgin A, Bernstein A, Trouard TP. A diffusion-matched principal component analysis (DM-PCA) based two-channel denoising procedure for high-resolution diffusion-weighted MRI. PLoS ONE **2018**; 13(4): e0195952.
16. Oguz I, Farzinfar M, Matsui J, et al. DTIPrep: quality control of diffusion-weighted images. Front Neuroinform **2014**; 8: 4.
17. Jenkinson M, Beckmann CF, Behrens TE, Woolrich MW, Smith SM. FSL. NeuroImage **2012**; 62(2): 782-90.
18. Smith RE, Tournier J-D, Calamante F, Connelly A. Anatomically-constrained tractography: improved diffusion MRI streamlines tractography through effective use of anatomical information. NeuroImage **2012**; 62(3): 1924-38.
19. Tournier JD, Calamante F, Connelly A. MRtrix: diffusion tractography in crossing fiber regions. International Journal of Imaging Systems and Technology **2012**; 22(1): 53-66.
20. Good CD, Johnsrude IS, Ashburner J, Henson RN, Friston KJ, Frackowiak RS. A voxel-based morphometric study of ageing in 465 normal adult human brains. Neuroimage **2001**; 14(1 Pt 1): 21-36.
21. Pruim RHR, Mennes M, van Rooij D, Llera A, Buitelaar JK, Beckmann CF. ICA-AROMA: A robust ICA-based strategy for removing motion artifacts from fMRI data. Neuroimage **2015**; 112: 267-77.

22. Andersson JLR, Jenkinson M, Smith S. Non-linear Registration, aka Spatial Normalisation. Oxford, United Kingdom: Oxford Centre for Functional MRI of the Brain, **2007**.

23. Taylor PA, Saad ZS. FATCAT: (an efficient) Functional and Tractographic Connectivity Analysis Toolbox. Brain Connect **2013**; 3(5): 523-35.

24. Zang Y, Jiang T, Lu Y, He Y, Tian L. Regional homogeneity approach to fMRI data analysis. Neuroimage **2004**; 22(1): 394-400.

25. Li YO, Adali T, Calhoun VD. Estimating the number of independent components for functional magnetic resonance imaging data. Hum Brain Mapp **2007**; 28(11): 1251-66.

26. Desikan RS, Ségonne F, Fischl B, et al. An automated labeling system for subdividing the human cerebral cortex on MRI scans into gyral based regions of interest. NeuroImage **2006**; 31(3): 968-80.

27. Zhang S, Arfanakis K. Evaluation of standardized and study-specific diffusion tensor imaging templates of the adult human brain: Template characteristics, spatial normalization accuracy, and detection of small inter-group FA differences. NeuroImage **2018**; 172: 40-50.

28. Sherman SM. Thalamic relays and cortical functioning. Prog Brain Res **2005**; 149: 107-26.

29. Su T, Caan MW, Wit FW, et al. White matter structure alterations in HIV-1-infected men with sustained suppression of viraemia on treatment. AIDS **2016**; 30(2): 311-22.

30. Li RL, Sun J, Tang ZC, Zhang JJ, Li HJ. Axonal chronic injury in treatment-naive HIV+ adults with asymptomatic neurocognitive impairment and its relationship with clinical variables and cognitive status. BMC Neurol **2018**; 18(1): 66.

31. Correa DG, Zimmermann N, Doring TM, et al. Diffusion tensor MR imaging of white matter integrity in HIV-positive patients with planning deficit. Neuroradiology **2015**; 57(5): 475-82.

32. Kallianpur KJ, Jahanshad N, Sailasuta N, et al. Regional brain volumetric changes despite 2 years of treatment initiated during acute HIV infection. AIDS **2020**; 34(3): 415-26.

33. Niendam TA, Laird AR, Ray KL, Dean YM, Glahn DC, Carter CS. Meta-analytic evidence for a superordinate cognitive control network subserving diverse executive functions. Cognitive, Affective, & Behavioral Neuroscience **2012**; 12(2): 241-68.

34. Jiang L, Zuo X-N. Regional homogeneity: a multimodal, multiscale neuroimaging marker of the human connectome. Neuro **2016**; 22(5): 486-505.

35. Hakkers CS, Arends JE, Barth RE, Du Plessis S, Hoepelman AIM, Vink M. Review of functional MRI in HIV: Effects of aging and medication. J Neurovirol **2017**; 23(1): 20-32.

36. Sanford R, Fernandez Cruz AL, Scott SC, et al. Regionally Specific Brain Volumetric and Cortical Thickness Changes in HIV-Infected Patients in the HAART Era. J Acquir Immune Defic Syndr **2017**; 74(5): 563-70.

37. Ances BM, Ortega M, Vaida F, Heaps J, Paul R. Independent effects of HIV, aging, and HAART on brain volumetric measures. J Acquir Immune Defic Syndr **2012**; 59(5): 469-77.

38. Ragin AB, Wu Y, Gao Y, et al. Brain alterations within the first 100 days of HIV infection. Ann Clin Transl Neurol **2015**; 2(1): 12-21.

39. Sui J, Jiang R, Bustillo J, Calhoun V. Neuroimaging-based Individualized Prediction of Cognition and Behavior for Mental Disorders and Health: Methods and Promises. Biol Psychiatry **2020**; In press.

40. Sui J, Qi S, van Erp TGM, et al. Multimodal neuromarkers in schizophrenia via cognition-guided MRI fusion. Nat Commun **2018**; 9(1): 3028.

## TABLES

**Table 1.** Sample characteristics by HIV status

| | HIV-positive N=59 | HIV-negative N=58 | Statistic | p-value |
|---|---|---|---|---|
| Age in years, M (SD) | 41.24 (8.54) | 37.84 (9.47) | t(115) =2.04 | .044 |
| Female gender, n (%) | 14 (23.73%) | 20 (34.48%) | $\chi(1)^2$ =1.64 | .200 |
| African-American race, n (%) | 45 (76.27%) | 38 (65.52%) | $\chi(1)^2$ =1.64 | .200 |
| Education in years, M (SD) | 14.08 (2.08) | 14.72 (2.14) | t(115) =1.64 | .104 |
| Nicotine use in past 30 days, n (%) | 22 (37.29%) | 10 (17.24%) | $\chi(1)^2$ =5.92 | .015 |
| Alcohol use in past 30 days, n (%) | 34 (57.63%) | 34 (58.62%) | $\chi(1)^2$ =0.01 | .913 |
| Marijuana use in past 30 days, n (%) | 12 (20.34%) | 11 (18.97%) | $\chi(1)^2$ =0.04 | .852 |
| Global cognitive function, M (SD) | 45.31 (6.47) | 49.15 (6.52) | t(115) =3.20 | .002 |

**Table 2.** Group comparison on component loading for $IC_{23}$

| | HIV-positive N=59 | HIV-negative N=58 | Statistic | p-value |
|---|---|---|---|---|
| Gray matter volume (GMV), M (SD) | 0.032 (0.0094) | 0.036 (0.0083) | F(1,115) =6.357 | .013 |
| White matter integrity (FA), M (SD) | 0.051 (0.0090) | 0.056 (0.0087) | F(1,115) =7.359 | .008 |
| Brain activity (ReHo), M (SD) | 0.091 (0.0088) | 0.092 (0.0094) | F(1,115) =.572 | .451 |

## FIGURE LEGENDS

**Fig.1** Flowchart of the MCCAR+JICA fusion pipeline. The preprocessed MRI features (i.e., ReHo from resting-state fMRI, GMV from T1w, and FA from DWI) are entered with global cognitive scores as the reference. After completing the cognition-guided fusion, component loadings and spatial maps for each modality are generated.

**Fig. 2** Illustration of the joint independent component for each MRI modality. The brain maps show the regions that comprise the multi-modal component with brain maps visualized at |Z| > 3.0. The ReHo map includes regions with positive activation (red) and negative activation, or deactivation (blue). The scatter plots to the right illustrate the correlation of the component loadings with cognitive performance (global T score).

Figure 1

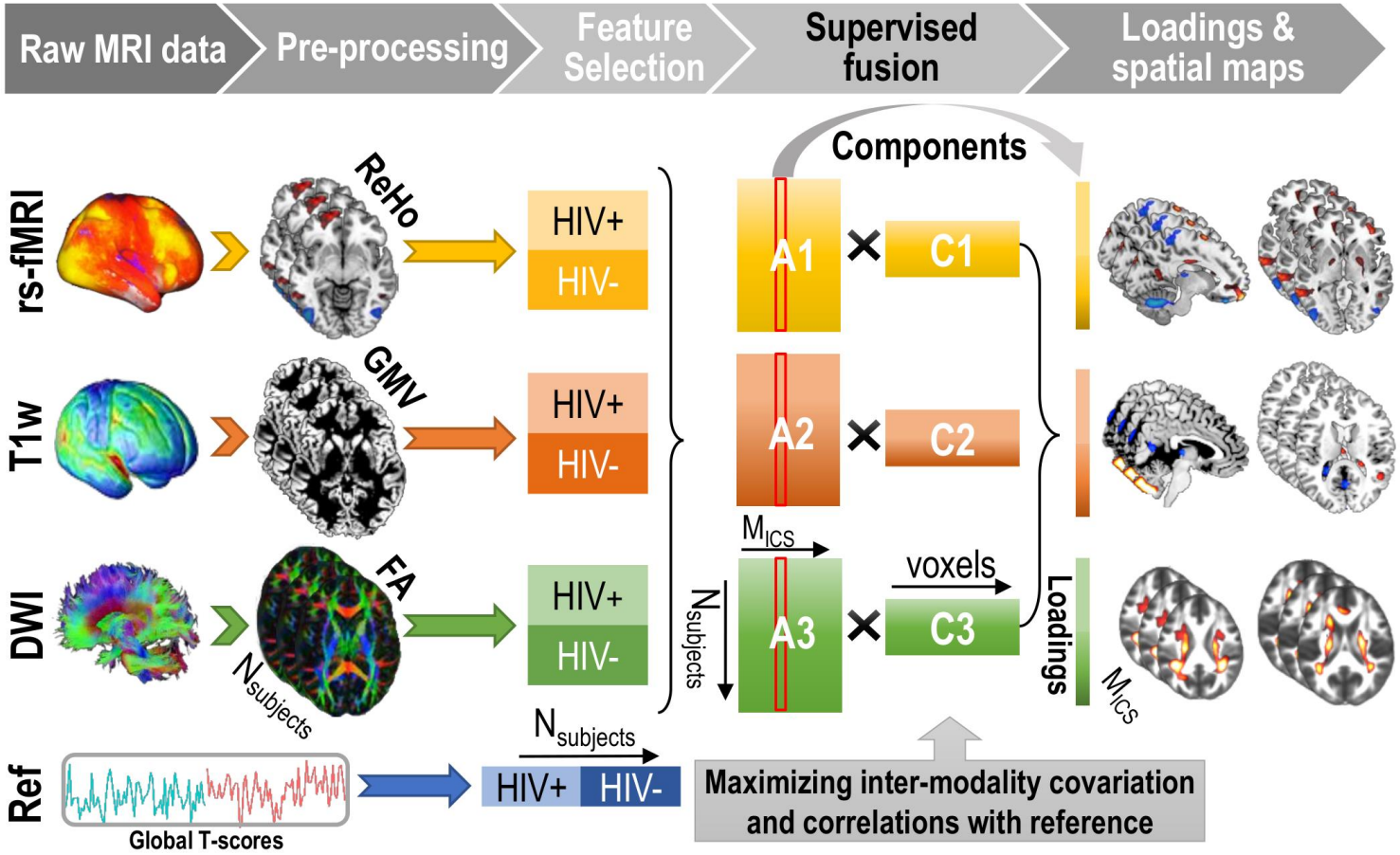

Figure 2